# Nonequilibrium Hypersonic Inviscid Steady Flows

M. Valorani,* M. Onofri,† B. Favini,‡ and F. Sabetta§
*Università degli Studi di Roma "La Sapienza," Rome, Italy*

**A numerical method for the solution of nonequilibrium flows about blunt bodies is presented. The method is based on the splitting in two parts of the reactive Euler equations: the gasdynamic operator (mass and momentum equations) and the chemical operator (energy and species conservation equations). The gasdynamic operator is discretized on a body- and shock-fitted grid, and integrated in diagonalized form by means of a semi-implicit technique. The chemical operator is integrated along the streamlines by means of an implicit technique with variable step size. A detailed chemical nonequilibrium model is adopted, while vibrational energy is assumed in equilibrium. The shock is modeled with a shock-fitting technique. Nonequilibrium flows about cylinders are computed in order to demonstrate the capability of the present method, both to achieve high resolution in chemical relaxation layers and to overcome the stiffness in near-equilibrium conditions without resulting in cumbersome calculations. Numerical results are presented and compared with experimental data.**

## I. Introduction

THE high temperatures generated behind the bow shock of blunt bodies traveling at hypersonic speed may yield nonequilibrium conditions, requiring the ideal gas model to be abandoned for a more appropriate one. In the temperature range typical of atmospheric re-entry problems, the main real gas effects are molecular dissociation and vibrational excitation, although other phenomena, such as ionization and electronic excitation, could be considered in order to improve the physical modeling.

The thickness of the layer where nonequilibrium effects show up is in general a fraction of the overall shock layer. Therefore, besides nonequilibrium regions, there are also regions where the flow may be assumed frozen or in near-equilibrium conditions. In general the extent of the different regions is not predictable a priori, and a nonequilibrium model has to be adopted even when the flow is in near-equilibrium conditions over most of the domain. As a consequence, the system of the governing equations may turn out to be stiff.[1] It is worthwhile to emphasize that in the present context the term "stiffness" should be used when referring not only to stability but also to accuracy. On the contrary, it is a common habit in the context of hypersonics to identify stiffness with the stability of the integration technique only (see, for example, Refs. 2 and 3).

For one-dimensional steady-state flows, a simple and efficient way to overcome the stiffness is to locally linearize the equations and then integrate the system by means of an implicit technique with variable step size.[4] When multidimensional problems are considered, the extension of this technique would require the solution of the fully coupled system of equations on an adaptive grid, which is a rather complex and expensive procedure. An alternative approach[5-7] is to split the system of equations into two parts: 1) a set consisting of the conservation of mass and momentum of the mixture, which is conventionally referred to as gasdynamic operator, and 2) a set consisting of the conservation equations of the mixture energy and of the mass of each species, denoted as chemical operator.

As far as dissociation reactions are considered, strong variations in temperature and species concentrations produce smoother gradients of pressure and fluid velocity, and the stiffness is mainly confined in the chemical operator.

In the present paper we take advantage of these properties by discretizing the two operators on two grids, differing both in structure and resolution, and then by integrating them using different techniques. The chemical operator written in steady-state form is integrated marching along the streamlines—where it reduces to a one-dimensional problem—by means of an implicit technique with self-adjusting integration step. For the gasdynamic operator we adopt the method proposed in Ref. 8, where the mass and momentum conservation equations are recast as compatibility equations and then solved on a body- and shock-fitted coordinate system, marching along the coordinate lines by means of a semi-implicit technique.

In the present model air is assumed to react at a finite rate, whereas thermal equilibrium is assumed for translation, rotation, and vibration. The assumption of vibrational equilibrium is somewhat restrictive, especially when the shock and the vibrational relaxation layers become of comparable width. However, a vibrational nonequilibrium model could be easily implemented into the proposed method.

In the next section, the nonequilibrium phenomenology is analyzed in more detail in order to point out the specific difficulties to be faced in the solution of hypersonic flows—difficulties typical of singularly perturbed problems. In Sec. III, the mathematical model is presented and a suitable set of dependent variables is chosen. In Sec. IV the integration techniques for the gasdynamic operator and the chemical operator are illustrated. In Sec. V the method used is applied to a test case of dissociating nitrogen about a cylinder,[9] and comparisons between experimental and numerical results are presented. Results for hypersonic air flows at different body sizes and freestream conditions are also reported.

## II. Nonequilibrium Effects and Nonequilibrium Model

From a mathematical point of view, the structure of the shock layer about a blunt body at high freestream Mach number is classifiable as a singularly perturbed problem with inner and outer solutions.[10-12]

The mathematical model for flows with finite-rate chemistry is provided by the laws of conservation of mass, momentum, and energy, plus a set of rate equations for the nonequilibrium processes. The system of equations is closed by an equation of

Presented as Paper 89-0671 at the AIAA 27th Aerospace Sciences Meeting, Reno, NV, Jan. 9-12, 1989; received March 19, 1989; revision received Aug. 31, 1990; accepted for publication Sept. 25, 1990.


*Ph.D. Student; currently Research Scientist, Dipartimento di Meccanica e Aeronautica. Member AIAA.
†Associate Professor, Dipartimento di Meccanica e Aeronautica. Senior Member AIAA.
‡Research Scientist, Dipartimento di Meccanica e Aeronautica.
§Full Professor, Dipartimento di Meccanica e Aeronautica.

state $h = h(p,T,Y)$, where $Y$ is a vector specifying the nonequilibrium state variables of the gas. Let us assume that only one nonequilibrium process occurs in the flow: a generalized rate equation (Ref. 10) may be written in nondimensional form as

$$\frac{1}{Da}\frac{DY}{Dt} = \frac{\chi}{\tau} \tag{1}$$

where $D/Dt$ denotes the substantial derivative, $\tau$ is the local relaxation time, and $\chi$ is a measure of the departure of the system from the equilibrium state $Y^*(p,T)$, which is implicitly defined by

$$\chi(p,T,Y^*) = 0 \tag{2}$$

$Da$ is the Damköhler number defined as the ratio between the flow time scale $\tau_f$ and the nonequilibrium process time scale $\tau_c$.

Two limiting regimes may be defined in terms of $Da$: the frozen limit for $Da \to 0$ and the equilibrium limit for $Da \to \infty$. In the latter limit, the coefficient of Eq. (1) vanishes, and a singular perturbation problem arises. The nonequilibrium model may then be substituted by an equilibrium model for which the first-order differential equation (1) is replaced by the algebraic equation (2).

In the case of the frozen limit, Eq. (1) has the solution $Y = \text{const}$ along trajectories, which simply states that no chemical activity occurs. In this limit the nonequilibrium model may be replaced by the standard inert gas model.

When dealing with flows around re-entry vehicles, the order of magnitude of the Damköhler number may be estimated on the basis of the freestream Mach number and of the body size. The Mach number determines the temperature behind the shock and hence sets a typical value of $\tau_c$; the body size and flow speed provide a typical value of $\tau_f$. The Damköhler number obtained in this way identifies only the regime prevailing in the flowfield, but all the above mentioned regimes can locally occur in actual flowfields.

For instance, if very large body sizes are considered ($Da \gg 1$), the flow is almost everywhere in equilibrium, but there is always a thin layer behind the shock where the flow is in nonequilibrium ($Da_{\text{loc}} \approx 1$). The thickness of this relaxation layer (an inner solution with respect to the outer equilibium flow) is of order $1/Da$. On the other hand, when small sizes of the body are considered, the flow is close to frozen conditions almost everywhere ($Da \ll 1$) except near the stagnation point, where it must always reach an equilibrium state ($Da_{\text{loc}} \gg 1$). These thin regions where large gradients of the chemical variables occur will be referred to as "chemical boundary layers."

Since it is not possible to predict exactly when and where the two limiting regimes will occur, the more general nonequilibrium model has to be adopted everywhere. However, the solution of this model gives rise to numerical difficulties when applied in regions of near equilibrium or in regions of chemical boundary layers.

As the equilibrium limit is approached, the differential equation (1) becomes stiffer and stiffer. If a linear multistep method is chosen to approximate Eq. (1), the stability requirements force the scheme to be implicit. This corresponds to following accurately only the slowly varying modes (driving modes corresponding to small eigenvalues) and to require that the rapidly damped modes (parasitic modes corresponding to large eigenvalues) remain stable. Nevertheless, the solution of the implicit scheme still presents some problems since "the stiffness of the original system of differential equations translates into ill-conditioning for the system of finite equations."[1] In fact, the condition number for the matrix $A$ associated with a discrete form of Eq. (1) is defined by

$$\mu(A) = \|A\| \cdot \|A^{-1}\|$$

and it is approximately equal to $|\lambda_m \lambda_1^{-1}|$, where $\lambda_1$ and $\lambda_m$ are respectively the smallest and largest eigenvalues of $A$. Hence, the stiffer the equation, the more ill-conditioned becomes the matrix, and appropriate numerical techniques must then be adopted.

On the other side, the problem in chemical boundary layers is to achieve a suitable resolution in order to accurately follow the nonlinearity of the solution.[4] As previously stated, boundary-layer type regimes may occur behind shock waves or when a flow under near frozen conditions approaches a stagnation point (the frozen limit).

In the frozen limit, the spatial gradients of some state variables (entropy, mass fractions, etc.) near a stagnation point grow steeper and steeper as the Damköhler number of the outer flow tends to zero. It has been demonstrated that, as $Da \to 0$, these gradients tend to infinity, and that this singularity has a nonanalytical behavior.[13,14] A physical description of this behavior may be the following: In the limiting process of $Da$ tending to zero, it is always possible to select a value of $Da$ small enough to make a flow particle approach the stagnation point closer and closer, still remaining in nearly frozen conditions. However, the particle will always reach an equilibrium state at the stagnation point, since there the flow time scale goes to infinity ($u \to 0$), while the chemical time scale remains finite. This transformation occurs in a vanishing small distance, which explains the occurrence of unbounded gradients. The equilibrium state at the stagnation point weakly depends on the actual value of the outer flow Damköhler number.

The other case of singularly perturbed behavior can occur behind a shock, which in nonequilibrium flows has a structure much more complicated than in the inert gas problem. A suitable model of this structure is the so-called partly dispersed shock[10,15] whose main assumptions are 1) across the shock, translational and rotational motions adjust so quickly that they can be considered in equilibrium, and 2) vibrational excitation and chemical reactions are much slower processes, and can be considered frozen across the shock. The transition from these conditions to the outer solution occurs in a layer that becomes thinner and thinner as the Damköhler number tends to infinity.

The solution of the relaxation layer behind the shock is deeply influenced by the discrete model chosen to describe the partly dispersed shock. An accurate and consistent way is to use a shock-fitting technique coupled with integration of the chemical operator along streamlines. The shock jump can be computed by assuming frozen chemistry and thermal equilibrium for translation and rotation; the frozen gas composition across the shock provides accurate initial conditions for the streamline integration of the chemical operator inside the relaxation layer.

The shock model used in the present work is slightly different from the classical partly dispersed model, since vibration is assumed to be in equilibrium. In particular, since in hypersonic flows the temperature behind the shock is so large that equilibrium vibrational energy is fully excited, modified Rankine-Hugoniot relations are used in which vibrational energy is zero ahead of the shock and equals $RT$ behind it.

## III. Mathematical Modeling

Once the shock is modeled by means of jump conditions, the governing equations for the smooth regions of the flowfield may be written in quasilinear form. Several quasilinear formulations may be considered, depending on the choice of dependent variables. In particular, the set $(p,h,q,Y)^T$ has been used by Rakich et al.[7] and by Botta et al.,[16] whereas the set $(a,s,q,Y)^T$ has been adopted by Onofri and Lentini.[17] In the present paper we select the second set of variables, which displays a lower degree of nonlinearity with respect to the first set, although it presents the drawback of introducing source terms in the momentum and energy equations.

The conservation equations for a reacting gas written in quasilinear form are

$$\frac{D\rho}{Dt} + \rho \nabla \cdot q = 0 \tag{3}$$

$$\frac{Dq}{Dt} + \frac{1}{\rho}\nabla p = 0 \tag{4}$$

$$\frac{De}{Dt} + p\frac{D(1/\rho)}{Dt} = 0 \tag{5}$$

$$\frac{DY}{Dt} = \hat{Y} \tag{6}$$

plus an equation of state $e = e(p,\rho,Y)$. The vector $Y$ represents the mass fractions of the different species, and $\hat{Y}$ is the vector of species production rates vector. To use a gasdynamic solver in terms of Riemann variables and entropy, the first term of Eq. (3) and the second of Eq. (4) must be expressed as functions of $s$, $Y$, and an auxiliary variable $\mathfrak{A}$, related to the frozen speed of sound $a$ through the relation

$$\mathfrak{A} = a/\delta \tag{7}$$

where $\delta = (\gamma - 1)/2$ and $\gamma$ is the ratio of specific heats of the gas mixture.

Using the thermodynamic relations for a mixture of gases and the Gibbs equation

$$T\,ds = de + p\,d(1/\rho) - \mu \cdot dY \tag{8}$$

where $\mu$ is a vector whose components are the chemical potentials, the following expressions, relating the differentials of $p$ and $\rho$ with those of $\mathfrak{A}$, $s$, and $Y$, may be obtained

$$\frac{1}{\rho}\frac{D\rho}{Dt} = \frac{1}{a}\frac{D\mathfrak{A}}{Dt} - \sum_i P_i \frac{DY_i}{Dt} \tag{9}$$

$$\frac{1}{\rho}\nabla p = a\nabla\mathfrak{A} - T\left(\nabla s + \sum_i Q_i \nabla Y_i\right) \tag{10}$$

where $P_i$ and $Q_i$ are defined as

$$P_i = \frac{1}{2\delta}\left[(\gamma+1)\frac{c_{p,i}}{c_p} - \gamma\frac{R_i}{R}\right] - \frac{e_i}{RT} \tag{11}$$

$$Q_i = c_p\left[(\gamma+1)\frac{c_{p,i}}{c_p} - \gamma\frac{R_i}{R}\right] - s_i \tag{12}$$

and $e_i$, $s_i$, $c_{p,i}$, $R_i$ are, respectively, internal energy, entropy, constant pressure specific heat, and the gas constant of each species; $e$, $s$, $c_p$, and $R$ are the same quantities for the gas mixture. All mixture properties per unit mass, say $f$, are expressed in terms of species properties $f_i$ by means of weighted averages

$$f = \sum_i f_i Y_i \tag{13}$$

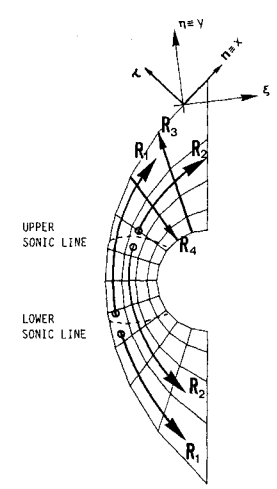


**Fig. 1 Directions of integration of Riemann variables.**

By means of Eq. (8), the energy conservation equation may also be written in terms of entropy, and the set of conservation laws becomes

$$\mathfrak{A}_{,t} + q \cdot \nabla\mathfrak{A} + a\nabla \cdot q = \hat{\mathfrak{A}} \tag{14}$$

$$q_{,t} + q \cdot \nabla q + a\nabla\mathfrak{A} = \hat{q} \tag{15}$$

$$s_{,t} + q \cdot \nabla s = \hat{s} \tag{16}$$

$$Y_{,t} + q \cdot \nabla Y = \hat{Y} \tag{17}$$

where the source terms $\hat{\mathfrak{A}}$, $\hat{q}$, $\hat{s}$ are given by

$$\hat{\mathfrak{A}} = a\sum_i P_i \frac{DY_i}{Dt}$$

$$\hat{q} = T\left(\nabla s + \sum_i Q_i \nabla Y_i\right)$$

$$\hat{s} = -(1/T)\mu \cdot \hat{Y} \tag{18}$$

The components of $\hat{Y}$ are defined as

$$\hat{Y}_i = \frac{w_i}{\rho}\sum_{k=1}^{m}\left\{(\nu''_{ik} - \nu'_{ik})\left[K_k^f \prod_{j=1}^{n}(c_j)^{\nu'_{jk}} - K_k^b \prod_{j=1}^{n}(c_j)^{\nu''_{jk}}\right]\right\} \tag{19}$$

where $\nu'_{ik}$, $\nu''_{ik}$ are, respectively, the reactants and products stoichiometric coefficients, $w_i$ is the molecular weight, $c_j$ are molar concentrations, $m$ is the number of reactions, and $n$ is the number of species.

For the $k$th reaction, the forward reaction coefficient $K_k^f$, the backward reaction coefficient $K_k^b$, and the equilibrium constant $K_k^e$ are given by

$$K_k^f = \beta_k T^{\alpha_k} \exp(-\theta_k/T)$$

$$K_k^b = K_k^f/K_k^e$$

$$K_k^e = \exp\left(\sum_{j=0}^{4} A_{jk}T^j\right) \tag{20}$$

The constants $\alpha_k$, $\beta_k$, $\theta_k$, and $A_{jk}$ may be found in Ref. 18.

## IV. Integration Technique

As said, an operator splitting between gasdynamics and chemistry has been adopted. The two operators, described in the following, are applied iteratively: the gasdynamic operator integrates the mass and momentum equations with entropy and concentrations frozen at the values determined in the previous iteration of the chemical operator; the chemical operator integrates the conservation equations of species and energy with frozen values of pressure and velocity.

### A. Integration of the Gasdynamic Operator

The integration domain, bounded by the bow shock, the body surface, and the supersonic outflow boundaries, is described by a nonorthogonal system of coordinate lines (Fig. 1). The mapping of the physical domain $(X,Y)$ onto the computational domain $(x,y)$ is obtained by a conformal mapping, followed by a stretching to fit the shock with a coordinate line. The two transformations are defined by

$$\xi = \arctan(Y/X)$$

$$\eta = \log(X^2 + Y^2)^{1/2} \tag{21}$$

and

$$x = \xi$$

$$y = \frac{\eta - b(\xi)}{z(t,\xi) - b(\xi)} \tag{22}$$

where $b(\xi)$ defines the body shape and $z(t,\xi)$ the shock in the $(\xi,\eta)$ plane.

As described in Ref. 8, it is possible to recast the mass and momentum conservation Eqs. (14) and (15) into four linearly dependent equations of compatibility, written along four orthogonal wave planes. The wave system, defined by the orthonormal versors $\boldsymbol{n}$ and $\boldsymbol{\tau}$, is oriented so that $\boldsymbol{n}$ is parallel to the shock and the body. As a consequence, $\boldsymbol{\tau}$ is normal both to the body and to the shock, which simplifies the implementation of the boundary conditions.

With $u$ and $v$ denoting the velocity components along $\boldsymbol{n}$ and $\boldsymbol{\tau}$, and with the introduction of the Riemann variables

$$R_1 = \mathfrak{A} + u, \quad R_2 = \mathfrak{A} - u, \quad R_3 = \mathfrak{A} + v, \quad R_4 = \mathfrak{A} - v \tag{23}$$

the compatibility equations become

$$R_{i,t} + \lambda_{ix} R_{i,x} + \lambda_{iy} R_{i,y} + \psi_i + \varphi_i = \hat{R}_i \qquad (i = 1,4) \tag{24}$$

where

$$\begin{aligned}
&\lambda_{1x} = x^n(u+a) + x^\tau v && \lambda_{1y} = y_{,t} + y^\tau v \\
&\lambda_{2x} = x^n(u-a) + x^\tau v && \lambda_{2y} = y_{,t} + y^\tau v \\
&\lambda_{3x} = x^n u + x^\tau(v+a) && \lambda_{3y} = y_{,t} + y^\tau(v+a) \\
&\lambda_{4x} = x^n u + x^\tau(v-a) && \lambda_{4y} = y_{,t} + y^\tau(v-a)
\end{aligned} \tag{25}$$

$$\begin{aligned}
&\psi_1 = a(x^\tau v_{,x} + y^\tau v_{,y}) && \varphi_1 = -vG_1 + aG_2 \\
&\psi_2 = a(x^\tau v_{,x} + y^\tau v_{,y}) && \varphi_2 = vG_1 + aG_2 \\
&\psi_3 = a x^n u_{,x} && \varphi_3 = uG_1 + aG_2 \\
&\psi_4 = a x^n u_{,x} && \varphi_4 = -uG_1 + aG_2
\end{aligned} \tag{26}$$

$$\begin{aligned}
\hat{R}_1 &= \left[a(x^n u + x^\tau v)\Sigma_i P_i + T x^n \Sigma Q_i\right] Y_{i,x} \\
&\quad + a y^\tau v \Sigma_i P_i Y_{i,y} + T x^n s_{,x} \\
\hat{R}_2 &= \left[a(x^n u + x^\tau v)\Sigma_i P_i - T x^n \Sigma Q_i\right] Y_{i,x} \\
&\quad + a y^\tau v \Sigma_i P_i Y_{i,y} - T x^n s_{,x} \\
\hat{R}_3 &= \left[a(x^n u + x^\tau v)\Sigma_i P_i + T x^n \Sigma Q_i\right] Y_{i,x} \\
&\quad + \left[a y^\tau v \Sigma_i P_i + T y^\tau \Sigma_i Q_i\right] Y_{i,y} + T(x^\tau s_{,x} + y^\tau s_{,y}) \\
\hat{R}_4 &= \left[a(x^n u + x^\tau v)\Sigma_i P_i - T x^n \Sigma Q_i\right] Y_{i,x} \\
&\quad + \left[a y^\tau v \Sigma_i P_i - T y^\tau \Sigma_i Q_i\right] Y_{i,y} - T(x^\tau s_{,x} + y^\tau s_{,y})
\end{aligned} \tag{27}$$

The metric coefficients are defined as follows:

$$\begin{aligned}
G_1 &= \alpha_{0,t} + u x^n \alpha_{0,x} + v(x^\tau \alpha_{0,x} + y^\tau \alpha_{0,y}) \\
G_2 &= v x^n \alpha_{0,x} + u(x^\tau \alpha_{0,x} + y^\tau \alpha_{0,y}) \\
x^n &= e^\eta \cos\alpha_2 \\
x^\tau &= -e^\eta \sin\alpha_2 \\
y^\tau &= \frac{e^\eta}{\cos\alpha_2} \frac{1}{c(t,\xi) - b(\xi)} \\
\alpha_0 &= \alpha_1 + \alpha_2 \\
\alpha_1 &= \arccos(\xi \cdot X) \\
\alpha_2 &= \arccos(\boldsymbol{n} \cdot \xi)
\end{aligned} \tag{28}$$

where $\xi$ and $X$ are the unit vectors associated with the directions of $\xi$ and $X$, respectively.

The four compatibility equations (24) are integrated independently of each other by means of a semi-implicit iterative technique.[8] The directions of sweeping are defined for each Riemann variable by the sign of the associated wave speed, i.e., $\lambda_{1x}$ for $R_1$, $\lambda_{2x}$ for $R_2$, $\lambda_{3y}$ for $R_3$, and $\lambda_{4y}$ for $R_4$. Therefore, $R_3$ is computed along $y$ lines from the body toward the shock, and vice versa for $R_4$. Since $\lambda_{1x}$ changes sign across the lower sonic line (see Fig. 1), $R_1$ is computed along $x$ lines starting from the sonic line and sweeping first toward the upper outflow boundary and then in the opposite direction toward the lower outflow boundary. The same holds symmetrically for $R_2$, starting from the upper sonic line.

In the compatibility equations (24), the terms containing the Riemann variables are discretized implicitly by a two-points upwind formula, according to the sign of $\lambda_{ix}$ and $\lambda_{iy}$. The same kind of upwinding is used in the evaluation of the derivatives appearing in the chemical source terms, whereas the derivatives in $\psi_i$ are discretized by a centered formula and the metric terms are evaluated analytically.

As mentioned, the particular choice of the $v$-component direction allows a very simple implementation of the boundary conditions. At the body surface the condition $v = 0$ provides the initial value $R_{3b} = R_{4b}$ for the integration of the $R_3$ equation. By this integration, the value $R_{3s}$ behind the shock is obtained. This allows determination of the relative Mach number normal to the shock, $M_n$, by solving the relation

$$\frac{R_{3s} - R_{3\infty}}{a_\infty} = \frac{1}{\delta}\left\{\frac{\left[(\gamma M_n^2 - \delta)(1 + \delta M_n^2)\right]^{1/2} + \delta(M_n^2 - 1)}{(1+\delta)M_n} - 1\right\} \tag{29}$$

Once $M_n$ is obtained, the kinematic and thermodynamic properties behind the shock, determined by means of the Rankine-Hugoniot relations, provide the initial value $R_{4s}$ for the integration of the $R_4$ equation. Based on $M_n$, the shock velocity and the new shock position are also computed. Then the grid is updated and the integration started again.

### B. Integration of the Chemical Operator

The chemical operator must provide the values of $s$ and $\boldsymbol{Y}$ at each node of the grid. The conservation equations for energy and chemical species, written in steady-state form, are

$$\boldsymbol{q} \cdot \nabla \boldsymbol{W} = \hat{\boldsymbol{W}}(p, \boldsymbol{W}) \tag{30}$$

where the vectors $\boldsymbol{W}$ and $\hat{\boldsymbol{W}}$ are defined as $\boldsymbol{W} = (s, \boldsymbol{Y})^T$ and $\hat{\boldsymbol{W}} = (\hat{s}, \hat{\boldsymbol{Y}})^T$, respectively. Since $\boldsymbol{q}$ is known from the previous iteration in the gasdynamic solver, it is possible to reconstruct the streamline passing through each grid point and to write Eq. (30) along the streamline as

$$\boldsymbol{W}_{,\sigma} = \boldsymbol{F}(p, q, \boldsymbol{W}) \tag{31}$$

where $\sigma$ is the curvilinear abscissa along the streamline.

Equation (31) can be integrated by a marching procedure once suitable initial values of $\boldsymbol{W}$ are assigned.

As said, stability may be assured by the use of an implicit scheme. The equation is discretized by means of a second-order box scheme

$$\Delta \boldsymbol{W} = \boldsymbol{W}_{n+1} - \boldsymbol{W}_n = (\Delta\sigma/2)(\boldsymbol{F}_{n+1} + \boldsymbol{F}_n) \tag{32}$$

where the source term $\boldsymbol{F}_{n+1}$ is locally linearized with respect to the dependent variables. Thus, Eq. (32) becomes

$$\left[1 - (\Delta\sigma/2)\boldsymbol{J}_n\right]\Delta \boldsymbol{W} = \Delta\sigma \boldsymbol{F}_n$$

where $\boldsymbol{J}$ is the Jacobian matrix of $\boldsymbol{F}$. The Jacobian $\boldsymbol{J}$ is evaluated numerically by means of finite differences. The size of the integration step $\Delta\sigma$ is varied according to the magnitude of $\Delta \boldsymbol{W}$ and $\Delta \boldsymbol{W}/\boldsymbol{W}$, following a criterion presented in Ref. 4.

The evaluation of the source term $\hat{\boldsymbol{Y}}$, whose components are given by Eqs. (19), requires the definition of a chemical kinet-

ics model. We have implemented the model proposed by Park,[18] which is based on five species ($O_2$, $N_2$, O, N, NO) and 17 reactions.

A critical point of the whole integration process is the choice of the starting values for $W$. The simplest way is to start the integration from the shock, where the frozen values of $Y$ and the values of $s$, given by the jump relations, are known exactly. However, this procedure is very time consuming since, for each grid point, the integration must be performed over the whole streamline, from the shock up to the grid point. A significant saving may be obtained if the integration is started from a point inside the flowfield, where the initial values for $W$ can be obtained by suitable interpolations. For instance, to compute $W$ at point A in Fig. 2, instead of starting from point K, it is possible to start from point C, where the values of $W$ are interpolated between B and D. The interpolation procedure reduces the accuracy in determining $W_A$ only slightly, provided that the $W$ field between B and D is smooth. Of course, this is not always the case, and if interpolation were used between points F and G to determine $W_E$, the error would be quite large due to the large $W$ gradients behind the shock. The procedure that has been adopted is based on a control of the $W$ gradient over the cell side intersected by the streamline. If this gradient is sufficiently small, interpolation is performed and the equations are integrated only along the streamline portion belonging to the cell. Otherwise, the streamline is reconstructed back to the shock and the integration is performed along the whole streamline.

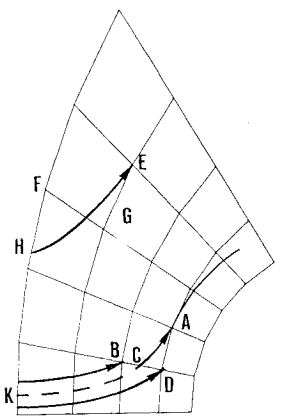


**Fig. 2 Sketch of streamline reconstruction.**

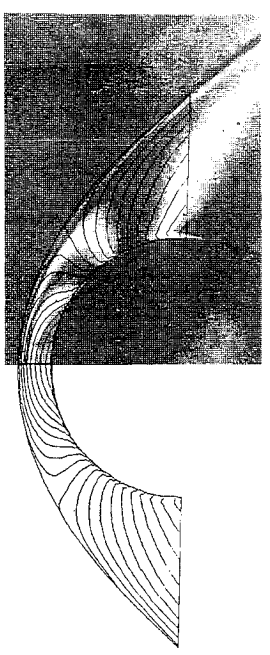

**Fig. 3 Isodensity lines with equilibrium vibration model, comparison with experimental results (Ref. 9).**

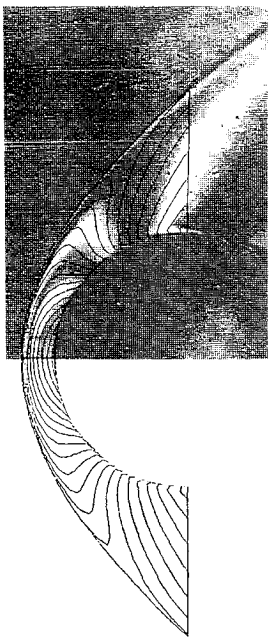

**Fig. 4 Isodensity lines with frozen vibration, comparison with experimental results (Ref. 9).**

## V. Results

To evaluate the reliability of the proposed model, the experimental conditions of Hornung[9] for the flow of partially dissociated nitrogen ($Y_{N_2}=0.927$, $Y_N=0.073$) over a 2-in.-diam cylinder have been adopted. The freestream conditions are $T_\infty=1833$ K, $p_\infty=2910$ Pa and $M_\infty=6.14$. The computed isodensity lines are compared in Fig. 3 with the constant fringe number contours of the interferogram by Hornung. It may be observed that the shock shape fits rather well the experimental one, and that the pattern of the isodensity lines agrees near the axis and over the outflow region. The disagreement in the region around 45 deg may be attributed to the assumption of vibrational equilibrium, which lowers the temperature too much just behind the shock, thus causing overprediction of density. If the vibrational energy is assumed to be frozen at the freestream value (i.e., no vibration), the pattern of the isodensity lines behind the shock becomes much more similar to the experimental one, as shown in Fig. 4. This confirms the statement by Candler[19] that a nonequilibrium model for vibration is needed in order to properly represent the flowfield about small bodies. However, the comparison of the two limiting cases of Figs. 3 and 4 indicates that the different assumptions on vibrational energy do not significantly affect the stand-off distance and the overall structure of the shock layer, in contrast with the result of Candler,[19] who claimed that the use of a one-temperature model would lead to a stand-off distance almost half of the actual one. Moreover, it must be pointed out that for body sizes typical of re-entry problems, the vibrational nonequilibrium is confined in a narrower layer behind the shock, and therefore, the error introduced by the vibrational equilibrium assumption becomes smaller.

The model has then been tested for more severe nonequilibrium conditions, such as those relevant to re-entry problems. The freestream gas is undissociated air at $T_\infty=205$ K, $p_\infty=2.05$ Pa, and the cylinder radius is $r=1$ m. A grid with $48\times16$ intervals has been used for all the presented computations.

When computing flows at very large freestream Mach number, the convergence of the iterative procedure between the chemical and the gasdynamic solvers requires appropriate ini-

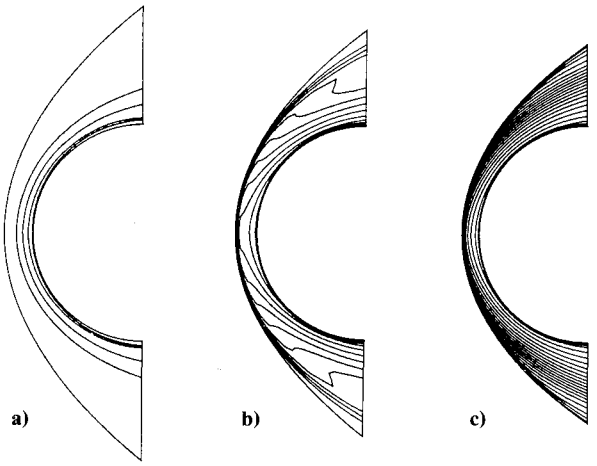


**Fig. 5 Isolines for $N_2$ concentration: a) $M_\infty = 13$, $Y_{min} = 0.73$, $Y_{max} = 0.77$; b) $M_\infty = 19$, $Y_{min} = 0.63$, $Y_{max} = 0.77$; and c) $M_\infty = 25$, $Y_{min} = 0.35$, $Y_{max} = 0.77$.**

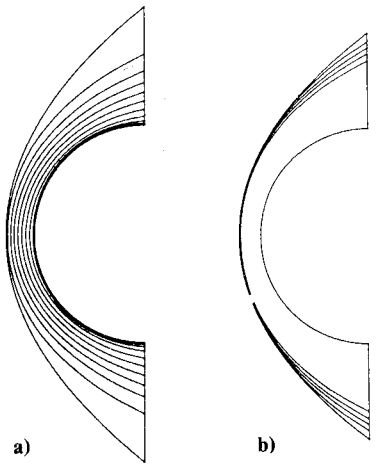


**Fig. 6 Isolines for $O_2$ concentration: a) $M_\infty = 13$, $Y_{min} = 0.045$, $Y_{max} = 0.23$; and b) $M_\infty = 19$, $Y_{min} = 0.6e^{-06}$, $Y_{max} = 0.23$.**

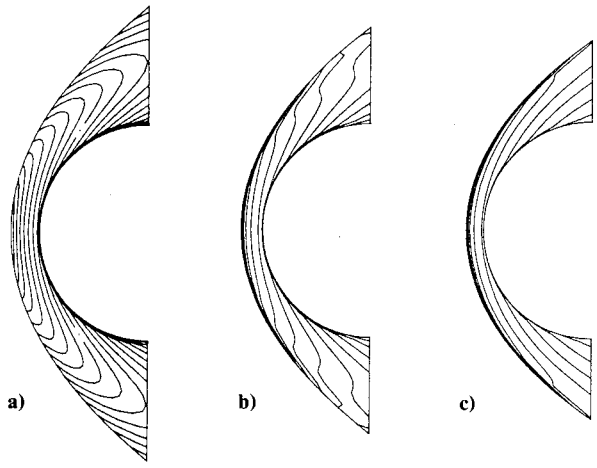


**Fig. 7 Isothermal lines: a) $M_\infty = 13$, $T_{max} = 5800$ K; b) $M_\infty = 19$, $T_{max} = 12{,}000$ K; and c) $M_\infty = 25$, $T_{max} = 20{,}000$ K.**

tial conditions. Since the concentration and temperature fields vary considerably at different values of $M_\infty$ (see Figs. 5–7), a rough initialization, like the one used for nonreacting flows, does not lead to convergence when computing flows in strong nonequilibrium. A suitable procedure is to start from a nonreacting solution at a lower freestream Mach number and to allow a gradual evolution of the flowfield, increasing progressively the freestream Mach number. Figure 8 shows the convergence of a solution for $M_\infty = 25$, which has been started with a nonreacting flowfield at $M_\infty = 13$. The velocity difference between two successive iterations of the gasdynamic solver times the entropy difference between two successive iterations of the chemical solver has been adopted as a measure of convergence. To reduce the error below $10^{-9}$, 1650 iterations of the gasdynamic solver and only 11 iterations of the chemical solver are required. This corresponds to a CPU time of 210 s on a IBM 3090/600.

As previously mentioned, for a given body size, the structure of the chemical field is rather different at different flight conditions (Figs. 5 and 6). For instance, at $M_\infty = 13$, the $O_2$ dissociation occurs gradually over the whole shock layer, but only a small amount of $N_2$ dissociates near the body surface. On the contrary, at $M_\infty = 19$, $O_2$ dissociates completely in a very thin layer behind the shock, whereas the $N_2$ dissociation occurs over the whole field, with steeper gradients behind the shock and at the body surface.

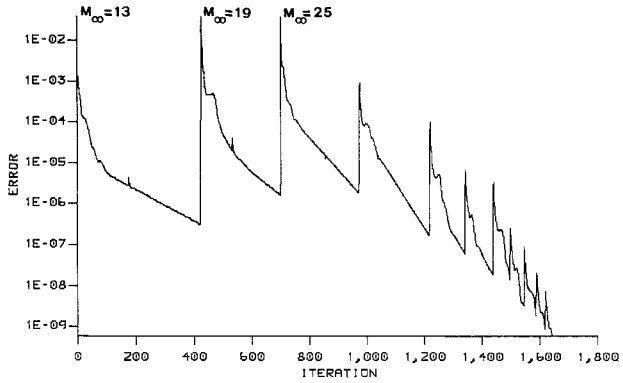


**Fig. 8 Convergence history.**

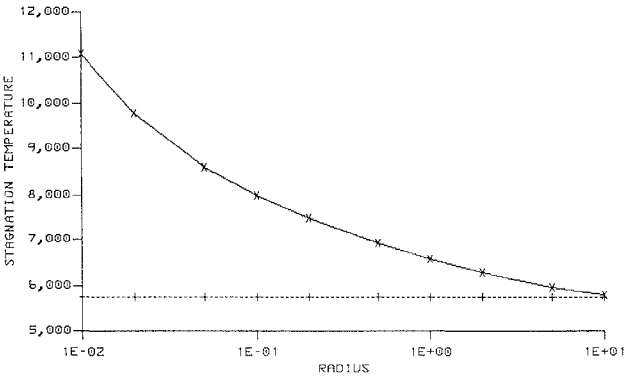


**Fig. 9 Stagnation temperature as function of cylinder radius: $M_\infty = 25$; —— × —— case A; − − − + − − − case B.**

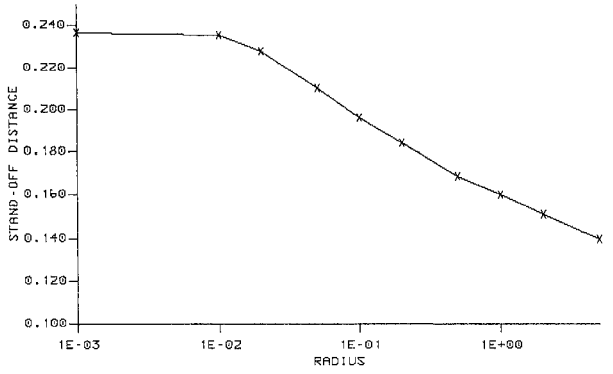


**Fig. 10 Nondimensional stand-off distance as function of cylinder radius: $M_\infty = 25$.**

The importance of an accurate calculation of these thin layers is emphasized by the results shown in Fig. 9, where, for different cylinder sizes, the temperature at the stagnation point has been computed using different integration steps for the chemical solver. In case A, approaching the stagnation point, the chemical integration step has the same size as the gasdynamic cell (1/16 of $r$), which would be the case if a fully coupled method were used. In case B, the integration of chemistry inside the last gasdynamic cell before the stagnation point is performed using 20 steps of diminishing size, with a quite negligible increase in computational cost.

For large body sizes ($r > 10$ m), the flow approaches the stagnation point in near-equilibrium conditions and there is not much difference in using either integration procedure. For smaller bodies (i.e., smaller $Da$), the outer flow is farther and farther from equilibrium, and approaches the frozen limit for $r \to 0$. In these cases, the procedure B is able to evaluate correctly the stagnation point equilibrium value, which, as stated by Conti and Van Dyke,[13] depends weakly on the outer flow Damköhler number. On the other hand, the procedure A drastically underpredicts $N_2$ dissociation, and this leads to stagnation temperatures twice as large as the actual equilibrium value. This result indicates that fully coupled solution methods can lead to significant overprediction of the stagnation temperature, unless very fine grids are assumed near the body surface.

The Damköhler number also influences significantly the topology of the shock layer. Figure 10 shows that the nondimensional stand-off distance varies by a factor of almost 2, approaching asymptotically the equilibrium value for $r \to \infty$ and the frozen value for $r \to 0$. Note that the frozen value is smaller than that for inert gas, since the equilibrium vibration is considered (see, also, Fig. 11). Moreover, the presence of thin nonequilibrium layers—behind the shock in the case $r \to \infty$ and near the body in the case $r \to 0$—affects the stand-off distance, which is slightly different from that computed with a frozen or an equilibrium flow model.

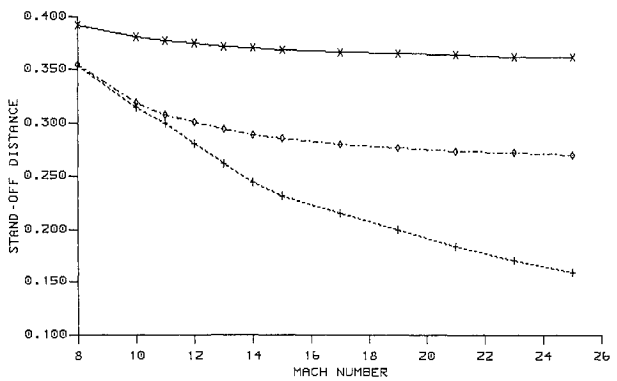


**Fig. 11 Nondimensional stand-off distance as function of $M_\infty$: $r = 1$ m; —— × —— inert gas; · — · — ◇ — · — · nonreacting gas and equilibrium vibration; — — — × — — — nonequilibrium chemistry and equilibrium vibration.**

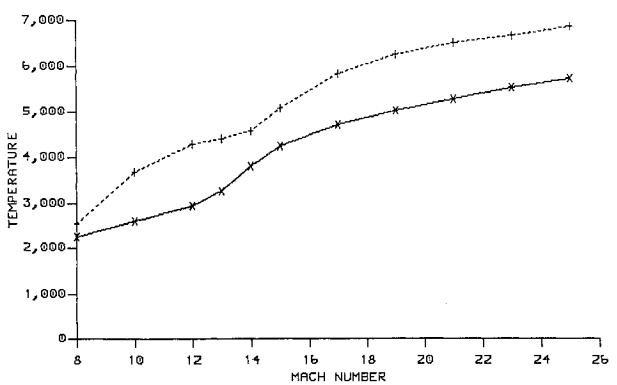


**Fig. 12 Stagnation temperature as function of $M_\infty$: $r = 1$ m; —— × —— stagnation temperature; --- + --- outer temperature.**

Finally, Figs. 11 and 12 report the behavior of the stand-off distance and of the stagnation temperature as a function of $M_\infty$ for a 1-m-radius cylinder. This corresponds again to considering flows at different $Da$, but in this case, keeping $\tau_f$ constant and varying $\tau_c$. In Fig. 11, the stand-off distance computed by the nonequilibrium model is compared with those obtained by an inert gas model and by a nonreacting model, including vibrational equilibrium. It is shown that, below $M_\infty = 10$, the influence of chemistry becomes negligible, although vibrational energy cannot be disregarded.

Figure 12 also reports the temperature at the last grid node before the stagnation point (the outer temperature). For $M_\infty \to 1$ and $M_\infty \to \infty$, the outer flow tends to equilibrium, and the outer temperature is slightly lower than the stagnation one. The positive difference between the outer and the stagnation temperatures may thus be considered a measure of the outer flow departure from equilibrium. Note that for $M_\infty = 14$ this difference attains a local minimum, since the $O_2$ dissociation is already in equilibrium, whereas $N_2$ dissociation is just starting. The results of Fig. 12 indicate that, for the range of body sizes and $M_\infty$ considered, nonequilibrium conditions always prevail inside the shock layer.

## VI. Conclusions

The proposed numerical model based on an operator splitting approach provides an effective method for the solution of hypersonic steady flows about blunt bodies. The operator splitting procedure allows the use of different integration techniques and different types of meshing for the gasdynamic and chemical operator. The method thus combines the high speed of convergence of the time-dependent implicit gasdynamic solver with the accuracy and stability of the steady implicit chemical operator.

The chemical operator is stable against the stiffness that develops in near equilibrium because of its implicit formulation, and it is accurate in the chemical boundary layers because of the use of a shock-fitting procedure and because of the integration along streamlines with self-adjusting step size. The latter feature becomes particularly effective in the solution of the flow singularity at the stagnation point.

The properties of fast convergence of the combined gasdynamic/chemical cycle have been numerically demonstrated.

Numerical predictions for the nitrogen flow about a cylinder compared against experimental results have been proved satisfactory. In particular, it has been verified that the one-temperature model for the chemical kinetics provides sufficiently accurate predictions, at least for the stand-off distance and the shock shape. However, the results also clearly show the influence, especially significant at small Damköhler numbers, of the vibrational nonequilibrium on the isodensity pattern.

The consistency of the results for hypersonic air flows has been positively checked over a wide range of Damköhler numbers. The importance of the variable step-size integration has been demonstrated by comparing the predictions of the stagnation conditions obtained with a coarse and a fine meshing along the stagnation streamline. The improved accuracy is obtained with a negligible increase of the computational cost.

## References

[1]Miranker, W. L., "Numerical Methods for Stiff Equations and Singular Perturbation Problems," *Mathematics and Its Application*, Vol. 5, D. Reidel Publishing Co., Dordrecht, The Netherlands, 1981, pp. 33–35.

[2]Li, C. P., "Implicit Methods for Computing Chemically Reacting Flow," NASA TM-58274, Sept. 1986.

[3]Gnoffo, P. A., McCandless, R. S., and Yee, H. C., "Enhancements to Program LAURA for Computation of Three-Dimensional

Hypersonic Flows," AIAA Paper 87-0280, Jan. 1986.
[4]Lomax, H., and Bailey, H. E., "A Critical Analysis of Various Integration Methods for Computing the Flow of a Gas in Chemical Nonequilibrium," NASA TN D-4109, Aug. 1967.
[5]Li, C. P., "Time-Dependent Solutions of Nonequilibrium Dissociating Gases Past a Blunt Body," *Journal of Spacecraft and Rockets,* Vol. 9, No. 8, 1972, pp. 571–572.
[6]Rizzi, A. and Bailey, H. E., "Reacting Nonequilibrium Flow Around the Space Shuttle Using a Time Split Method," *Proceedings of the NASA Conference on Aerodynamic Analyses Requiring Advanced Computers,* NASA SP-347, March 1975.
[7]Rakich, J. V., Bailey, H. E., and Park, C., "Computation of Nonequilibrium, Supersonic Three-Dimensional Inviscid Flow over Blunt-Nosed Body," *AIAA Journal,* Vol. 21, No. 6, 1983, pp. 834–841.
[8]Onofri, M., and Lentini, D., "Fast Numerical Solver for Transonic Flows," *Computers & Fluids,* Vol. 17, No. 1, 1989, pp. 195–204.
[9]Hornung, H. G., "Non-equilibrium Dissociating Nitrogen Flow over Spheres and Circular Cylinders," *Journal of Fluid Mechanics,* Vol. 53, Part I, 1972, pp. 149–176.
[10]Vincenti, W., and Kruger, C., *Introduction to Physical Gasdynamics,* Wiley, New York, 1967.
[11]Sedney, R. "Method of Characteristics," *Nonequilibrium Flows,* Vol. 2, edited by P. Wegener. M. Dekker, Inc., New York, 1969.
[12]Van Dyke, M., *Perturbation Methods in Fluid Mechanics,* Parabolic Press, Stanford, CA, 1975.
[13]Conti, R., and Van Dyke, M., "Inviscid Reacting Flow Near a Stagnation Point," *Journal of Fluid Mechanics,* Vol. 35, 1969, pp. 799–813.
[14]Vinokur, M., "On the Stagnation-Point Conditions in Nonequilibrium Inviscid Blunt Body Flows," *Journal of Fluid Mechanics,* Vol. 43, Part I, 1970, pp. 49–75.
[15]Zel'dovich, Y. B., and Raizer Y. P.,"Physics of Shock Waves and High-Temperature Hydrodynamic Phenomena," Vol. 2, Academic Press, New York, 1967.
[16]Botta, N., Pandolfi, M., and Germano, M., "Nonequilibrium Reacting Hypersonic Flow About Blunt Bodies, Numerical Prediction," AIAA Paper 88-0514, Jan. 1988.
[17]Onofri, M., and Lentini, D., "Inviscid Hypersonic Blunt Body Flows with Finite-Rate Chemical Kinetics," *7th GAMM Conference on Numerical Methods in Fluid Mechanics,* Louvaine-La-Neuve, Belgium, 1987, *Notes on Numerical Fluid Mechanics,* Vol. 20, edited by M. Deville, Vieweg, Braunschweig, Germany, 1988.
[18]Park, C., "On Convergence of Chemically Reacting Flows," AIAA Paper 85-0247, Jan. 1985.
[19]Candler G., "On the Computation of Shock Shapes in Nonequilibrium Hypersonic Flows," AIAA Paper 89-0312, Jan. 1989.